crystals

MDPI

Article

{Ca, Eu, Yb}$_{23}$Cu$_7$Mg$_4$ as a Step towards the Structural Generalization of Rare Earth-Rich Intermetallics

Pavlo Solokha, Riccardo Freccero and Serena De Negri *

Dipartimento di Chimica e Chimica Industriale, Università degli Studi di Genova, via Dodecaneso 31, 16146 Genova, Italy; pavlo.solokha@unige.it (P.S.); riccardo.freccero@unige.it (R.F.)
* Correspondence: serena.denegri@unige.it

Abstract: The $R_{23}Cu_7Mg_4$ (R = Ca, Eu) intermetallics, studied by single-crystal X-ray diffraction, were found to be isostructural with the $Yb_{23}Cu_7Mg_4$ prototype (*hP*68, k^4h^2fca, space group $P6_3/mmc$), forming a small group inside the bigger 23:7:4 family, otherwise adopting the *hP*68-$Pr_{23}Ir_7Mg_4$ crystal structure. The observed structural peculiarity is connected with the divalent character of the R component and with a noticeable volume contraction, resulting in the clear clustering of title compounds inside the whole 23:7:4 family. The occurrence of fragments typical of similar compounds, particularly Cu-centered trigonal prisms and Mg-centered core–shell polyicosahedral clusters with R at vertices, induced the search of significant structural relationships. In this work, a description of the hexagonal crystal structure of the studied compounds is proposed as a linear intergrowth along the c-direction of the two types of slabs, $R_{10}CuMg_3$ (parent type: *hP*28-kh^2ca, SG 194) and $R_{13}Cu_6Mg$ (parent type: *hR*60-b^6a^2, SG 160). The ratio of these slabs in the studied structure is 2:2 per unit cell, corresponding to the simple equation, $2 \times R_{10}CuMg_3 + 2 \times R_{13}Cu_6Mg = 2 \times R_{23}Cu_7Mg_4$. This description assimilates the studied compounds to the {Ca, Eu, Yb}$_4$CuMg ones, where the same slabs (of $p3m1$ layer symmetry) are stacked in a different way/ratio and constitutes a further step towards a structural generalization of R-rich ternary intermetallics.

Keywords: Mg-containing intermetallics; rare earth metals; polyicosahedral units; linear intergrowth concept; volume effects; structural generalization

Citation: Solokha, P.; Freccero, R.; De Negri, S. {Ca, Eu, Yb}$_{23}$Cu$_7$Mg$_4$ as a Step towards the Structural Generalization of Rare Earth-Rich Intermetallics. *Crystals* **2024**, *14*, 156. https://doi.org/10.3390/cryst14020156

Academic Editor: Andrey Prokofiev

Received: 22 December 2023
Revised: 28 January 2024
Accepted: 29 January 2024
Published: 31 January 2024

1. Introduction

The component interaction in RTX intermetallic systems (R = rare earth metal; T = transition metal; X = other metal) results in many ternary compounds with recurrent stoichiometries in different concentration ranges. These compounds have been widely studied both for their applicative and fundamental properties [1–12], and they represent an ever-growing database for studying structural relationships, aiming for simplified descriptions and rational generalizations.

The families of rare, earth-rich RTX representatives are highly populated, especially for R_4TX and $R_{23}T_7X_4$ stoichiometries, of which are each characterized by two different crystal structures (see Figure 1).

In the framework of a recent investigation on the R_4TX family, the new {Ca,Eu,Yb}$_4$CuMg compounds (*hR*144) were discovered and structurally elucidated in terms of an intergrowth concept [13].

As a logical evolution of this research, our attention focused on the $R_{23}T_7X_4$ family, mostly showing the *hP*68-$Pr_{23}Ir_7Mg_4$ structure [14]; an overview of chemical compositions of the currently known members is presented in Figure 2. This periodic table map shows that the components of these phases are light trivalent rare earth metals (R with Z < 65), late transition elements from 8 to 10 groups (T) and Mg, Zn, Cd or In (X). As derived from the expanded table in Figure 2b, the Mg- and Cd-containing groups are the most abundant; Zn and In having only one representative each, in combination with Ce and Ru.

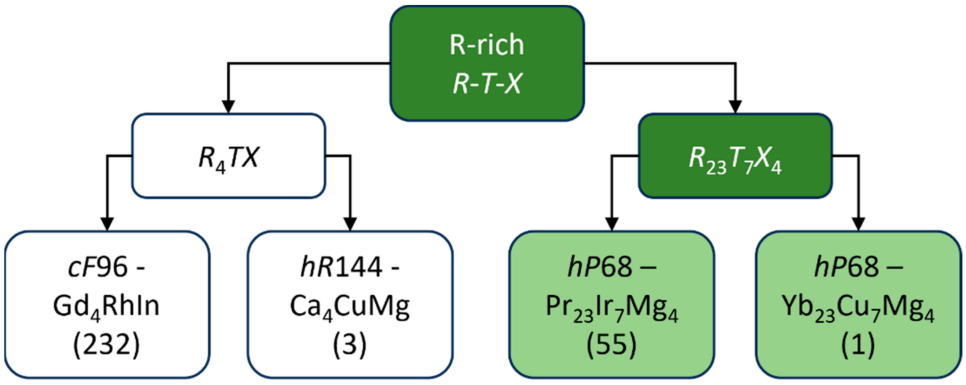

Figure 1. Crystal structures of the two most populated families of *R*-rich *RTX* intermetallics. Numbers of representatives are indicated in parentheses [4]. The green background highlights the object of the current investigation.

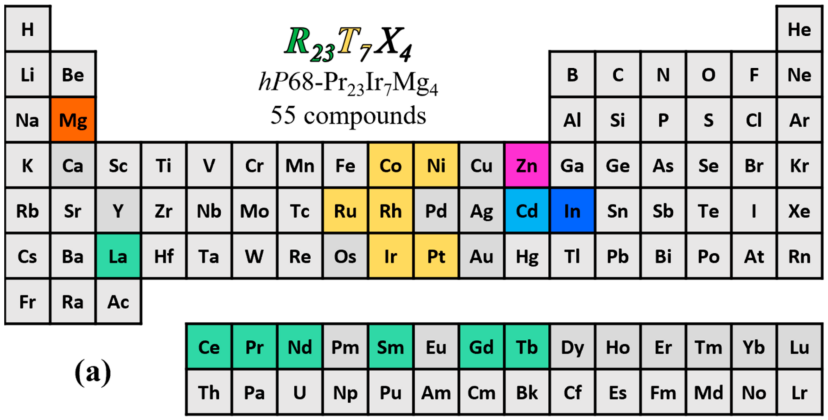

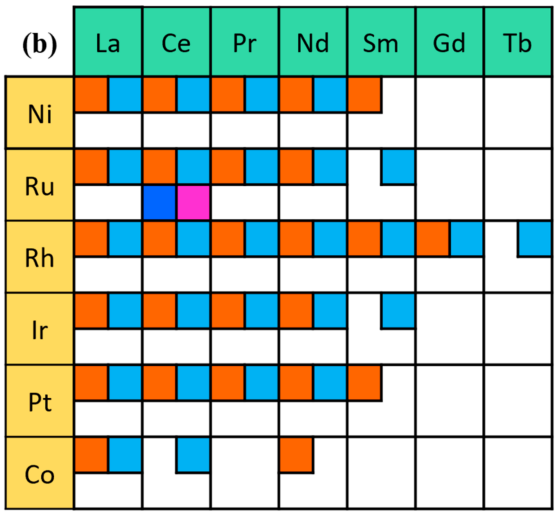

Figure 2. Constituents distribution among the $R_{23}T_7X_4$ family of compounds (*hP*68-$Pr_{23}Ir_7Mg_4$): (**a**) elements involved mapped on a periodic table; (**b**) expanded table representing specific ternary combinations. The coloring scheme is the same for both tables.

The *hP*68-$Yb_{23}Cu_7Mg_4$ structure is only represented by the prototype [15], thus it was decided to perform some explorative syntheses on divalent *R* analogues (*R* = Ca, Eu) with the aim to enrich this family and look for meaningful structural and chemical generalization criteria.

2. Experimental Section

Samples of the nominal composition $Ca_{67.6}Cu_{20.6}Mg_{11.8}$ (total mass = 0.5 g) and $Eu_{66.7}Cu_{20.3}Mg_{13}$ (total mass = 0.8 g) were prepared from pure (>99.9 mass %) components. The starting metals were weighted in stoichiometric amounts and placed in tantalum crucibles, arc sealing their cap to prevent Mg evaporation. These operations were performed in a glove box filled with Ar, to minimize side reactions with oxygen and water. The Ta crucibles were put in a quartz glass tube sealed under an inert atmosphere, then placed in a resistance furnace where the following thermal cycle was applied: 20 °C → (5 °C/min) → 850 °C (10 min) → (−0.1 °C/min) → 400 °C (5 min) → (−0.2 °C/min) → 100 °C (furnace switched off).

For microscopic characterization, some pieces of each sample were selected and embedded in a conductive phenolic resin and polymerized in a hot mounting press machine Opal 410 (ATM GmbH, Blieskastel, Germany). The surfaces were smoothed by SiC abrasive papers with no lubricant and polished with the aid of diamond pastes with particle size decreasing from 6 to 1 µm, using petroleum ether as lubricant. The automatic polishing machine Saphir 520 (ATM GmbH, Blieskastel, Germany) was applied for this purpose.

Microstructure observations, together with qualitative and quantitative analyses, were conducted on a Zeiss Evo 40 Scanning Electron Microscope (SEM) equipped with a Dispersive X-ray Spectroscopy (EDXS) system (INCA X-ACT), managed by the INCA Suite software version 4.15 (Oxford Instruments, Analytical Ltd., Bucks, UK). Both samples showed a good yield of the compound of interest, with an average composition of ~67 at.% *R*, 20 at.% Cu, 13 at.% Mg (see Figure 3), and were therefore subjected to X-ray diffraction studies. X-ray Powder Diffraction (XRPD) patterns were recorded on a X'Pert MPD diffractometer (Philips, Almelo, Netherlands) (Cu K_α radiation, step mode of scanning) and indexed using Powder Cell [16] software (version 2.4).

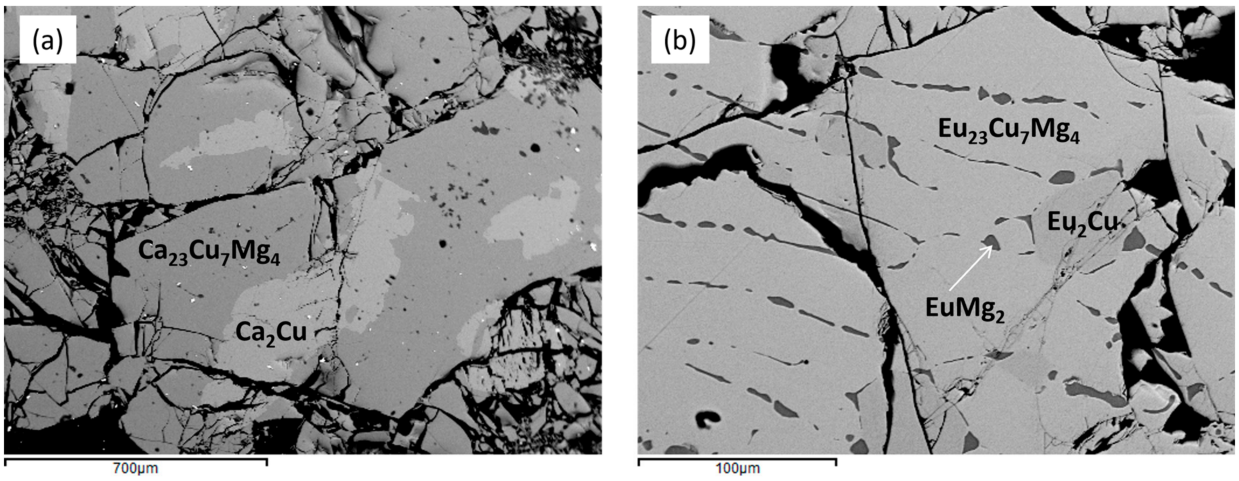

Figure 3. SEM images (BSE mode) of Ca-Cu-Mg (**a**) and Eu-Cu-Mg (**b**) samples. The phases detected by EDXS analysis are indicated.

Good-quality single crystals were selected with the help of a light microscope from mechanically crushed alloys covered with mineral oil. Crystals, embedded in an excess of grease to prevent oxidation, were then glued to pins and remained stable for several days.

The X-ray diffraction data were collected on a three-circle Bruker D8 QUEST diffractometer, equipped by a PHOTON III 14 photon-counting detector, using the graphite monochromatized Mo Kα radiation. Data collection strategies, consisting of both ω- and φ-scans, were decided using the APEX4 software (version 2022.10-1) [17] to obtain good data completeness, redundancy, and resolution limit. Data were collected over the reciprocal space up to ~31° in θ (resolution of ca. 0.7 Å) with exposures of 30–40 s per frame. The software SAINT (version 8.30) [18] and XPREP [19] were used for data reduction. Lorentz,

polarization, and absorption effects were corrected by SADABS [20]; the crystal structure was solved and refined with the aid of SHELXTL [21].

Both crystals possess hexagonal symmetry, and their diffraction patterns show systematic absences due to the presence of a *c*-type glide plane. Reconstructed intensity profiles of the selected zones are shown in Figure 4 for the Eu-compound diffraction pattern.

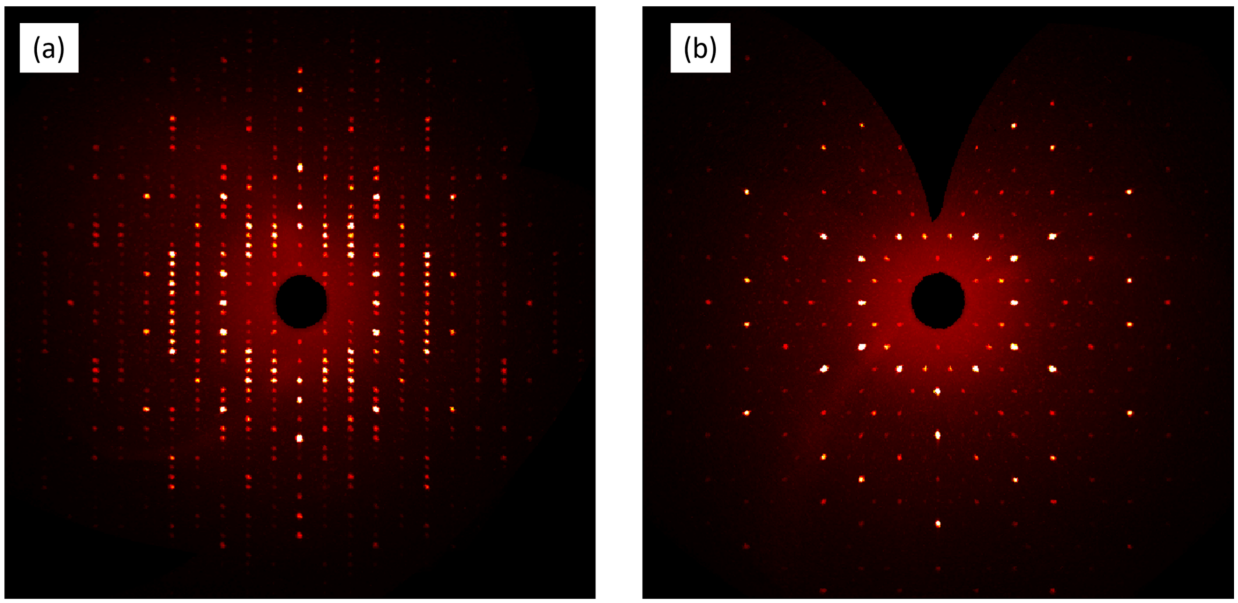

Figure 4. Reconstructed precession images of *h*0*l* (**a**) and *hk*0 (**b**) zones for the $Eu_{23}Cu_7Mg_4$.

The best structural model was found using the intrinsic phasing method in the $P6_3/mmc$ space group (N. 194), corresponding to the *hP*68-$Yb_{23}Cu_7Mg_4$ prototype. The unit cell, containing 2 formula units of $R_{23}Cu_7Mg_4$ composition, accounts for 68 atoms, distributed among 5 Wyckoff sites of *R*, 2 sites of Cu, and 2 of Mg. In the case of $Ca_{23}Cu_7Mg_4$, the first refinement resulted in somewhat high isotropic displacement parameters for Mg atoms in the 2*a* position. A Mg/Ca statistical mixture was refined for this site, resulting in 0.93/0.07 ratio and significantly improving residuals. For the Eu representative, no need for the statistical mixture was evidenced, and the structural model turned out to be perfectly stoichiometric. The final anisotropic full-matrix least-squares refinements converged to good residuals for both compounds. Details of data collection and the structure refinement are summarized in Table 1, together with selected crystal data; standardized atomic coordinates, site occupancy factors, and equivalent displacement parameters are listed in Table 2. The corresponding CIF files, available as Supplementary Materials, were deposited at the Cambridge Database.

Table 1. Selected crystallographic data and structure refinement parameters for the single crystals studied in this work.

Formula	$Ca_{22.93\ (4)}Cu_7Mg_{4.07\ (4)}$	$Eu_{23}Cu_7Mg_4$
EDXS composition	$Ca_{68.2}Cu_{19.8}Mg_{12.0}$	$Eu_{66.2}Cu_{19.2}Mg_{14.6}$
Depositing CSD-code	2266948	2266951
Formula weight (g/mol)	1463.86	4037.10
Space group	$P6_3/mmc$ (194)	
Pearson symbol-protoype, Z	*hP*68-$Yb_{23}Cu_7Mg_4$, 2	
a, Å	10.236 (2)	10.659 (2)

Table 1. *Cont.*

c, Å	23.413 (5)	24.379 (5)
V, Å^3	2124.5 (9)	2398.7 (10)
Calc. density (g·cm^{-3})	2.29	5.59
Absorption coefficient (μ, mm^{-1})	6.27	32.61
Theta range (°)	$2.3 \leq \theta \leq 33.2$	$2.8 \leq \theta \leq 30.5$
Index ranges *h*, *k*, *l*	$-15 \leq h \leq 11$ $-15 \leq k \leq 14$ $-36 \leq l \leq 35$	$-15 \leq h \leq 15$ $-15 \leq k \leq 13$ $-34 \leq l \leq 34$
Data/parameters	1592/41	1435/40
GOF	1.16	0.98
R_{int}/R_{sym}	0.1014/0.045	0.083/0.018
$R1/wR2$ ($I > 2\sigma(I)$)	0.0403/0.0932	0.0259/0.0454
$R1/wR2$ (all data)	0.0864/0.1320	0.0445/0.0524
Max diff. peak and hole (e$^-$/Å^3)	1.19 and −1.40	2.59 and −1.36

Table 2. Standardized atomic coordinates and equivalent displacement parameters (U_{eq}) for the {Ca, Eu}$_{23}$Cu$_7$Mg$_4$ single crystals.

Atom	**Site**	**Atomic Coordinates**			U_{eq} [Å^2]
		x/a	**y/b**	**z/c**	
$Ca_{22.93(4)}Cu_7Mg_{4.07(4)}$					
Ca1	4*f*	1/3	2/3	0.61757 (8)	0.0180 (4)
Ca2	12*k*	0.20651 (6)	0.4130 (1)	0.03215 (5)	0.0209 (2)
Ca3	6*h*	0.12164 (9)	0.24328 (9)	1/4	0.0211 (3)
Ca4	12*k*	0.12389 (6)	0.2478 (1)	0.61877 (5)	0.0219 (2)
Ca5	12*k*	0.53951 (6)	0.07902 (6)	0.66824 (5)	0.0217 (2)
Cu1	12*k*	0.52555 (4)	0.05110 (4)	0.04959 (3)	0.0243 (2)
Cu2	2*c*	1/3	2/3	1/4	0.0277 (4)
Mg1 (Ca) SOF(Mg) = 0.93	2*a*	0	0	0	0.0234 (17)
Mg2	6*h*	0.7706 (1)	0.5412 (3)	1/4	0.0190 (5)
$Eu_{23}Cu_7Mg_4$					
Eu1	4*f*	1/3	2/3	0.61610 (3)	0.0221 (2)
Eu2	12*k*	0.20717 (3)	0.41434 (5)	0.03062 (2)	0.0244 (1)
Eu3	6*h*	0.12316 (4)	0.24632 (4)	1/4	0.0264 (1)
Eu4	12*k*	0.12549 (3)	0.25099 (5)	0.61768 (2)	0.0277 (1)
Eu5	12*k*	0.53839 (2)	0.07678 (2)	0.66768 (2)	0.0240 (1)
Cu1	12*k*	0.52492 (6)	0.04984 (4)	0.04907 (6)	0.0308 (3)
Cu2	2*c*	1/3	2/3	1/4	0.0311 (6)
Mg1	2*a*	0	0	0	0.0255 (6)
Mg2	6*h*	0.76850 (2)	0.53700 (5)	1/4	0.0254 (9)

3. Results and Discussion

The studied {Ca, Eu}$_{23}$Cu$_7$Mg$_4$ compounds, together with the Yb-containing prototype, form a small sub-family of $R_{23}T_7X_4$, with a crystal structure (*hP*68-Yb$_{23}$Cu$_7$Mg$_4$, Wyckoff sequence k^4h^2fca, see Table 2) different from all of the others (*hP*68-Pr$_{23}$Ir$_7$Mg$_4$, Wyckoff sequence $c^{10}b^2a^2$); however, having in common with all of them is the hexagonal symmetry and the number of atoms in the unit cell.

A first glance to the crystal structures of interest, in terms of interatomic distances, shows that the *R*–Mg (3.52 ÷ 3.74 Å for Ca, 3.69 ÷ 3.90 Å for Eu), Cu–Cu (2.49 for Ca, 2.56 for Eu), and Mg–Mg (3.19 for Ca, 3.26 for Eu) contacts are compatible with the metallic radii sums [22]; instead Mg and Cu are well apart and do not interact. Also, the first coordination spheres of the different species are geometrically similar to those in other *RTX* compounds rich in *R*. These polyhedra are capped Cu-centered trigonal prisms, either isolated (Cu@*R*(6 + 3)) or sharing a rectangular face (Cu@Cu*R*(6 + 2)), isolated Mg-centered icosahedra (Mg@*R*12), and polyicosahedral Mg3@*R*20 core–shell clusters (see Figure 5).

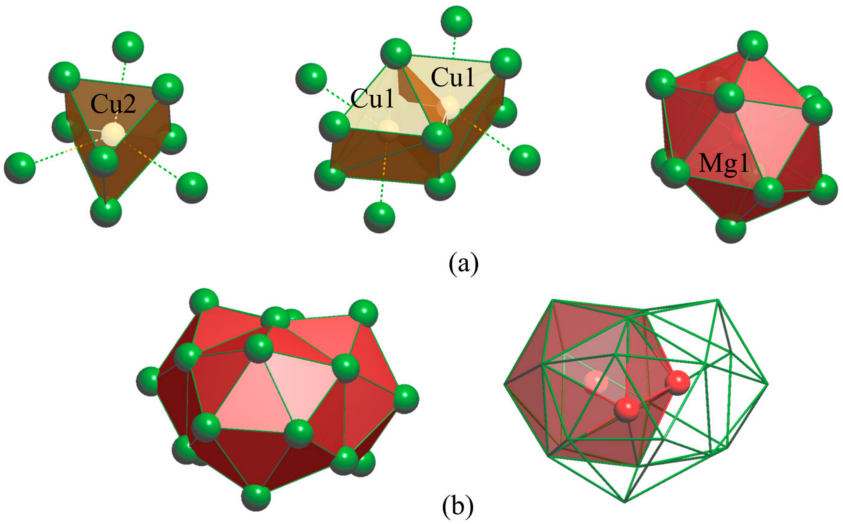

Figure 5. Characteristic structural fragments of {Ca, Eu, Yb}$_{23}$Cu$_7$Mg$_4$ compounds. (**a**) coordination polyhedra for Cu and Mg1 species; (**b**) Mg3@R20 polyicosahedral cluster (Mg2 species) with closed (**left**) and open/transparent (**right**) faces.

The same coordination polyhedra were observed in R_4CuMg (*R* = Ca, Eu, Yb) compounds [13], with a difference in the Mg-centered polyicosahedral units; in the 23:7:4, these are formed by three fused icosahedra, instead in the 4:1:1, six fused icosahedra form core–shell clusters of the Mg7@*R*32 composition. Recently, we proposed an elegant description of the R_4CuMg structure in terms of the linear intergrowth of slabs of $R_{9.5}$CuMg$_{3.5}$ and R_{13}Cu$_6$Mg composition [13]. Considering the cited similarities, an analogous description was attempted with success also for R_{23}Cu$_7$Mg$_4$ with the divalent *R*.

In fact, the structure of title compounds can be interpreted as a stacking of slabs from the same parent structures that have been extensively described in [13]: the hexagonal *hP*28-kh^2ca (SG 194) adopted by many R_9TX_4 and $R_{10}TX_3$ compounds and the rhombohedral *hR*60-b^6a^2 (SG 160) only adopted by Lu$_{13}$Ni$_6$In [23]. Slabs of each parent type are alternatively stacked along the *c*-direction, fulfilling the crystal space with no gaps neither need of "gluing" atoms (see Figure 6a). Slabs, possessing the same *p*3*m*1 layer symmetry, are joined by a common corrugated layer composed exclusively by *R* atoms, showing two types of nodes represented by $(3^6)^1$, $(3^2434)^6$ Schläfli notation (see Figure 6b).

As a consequence of this, the composition of the slabs from the hexagonal parent type is R_{10}CuMg$_3$, and instead the composition of the other slabs is exactly R_{13}Cu$_6$Mg. Therefore, the 23:7:4 unit-cell content can be easily described by properly considering the composition and number of stacked slabs: 2 × R_{10}CuMg$_3$ + 2 × R_{13}Cu$_6$Mg = 2 × R_{23}Cu$_7$Mg$_4$.

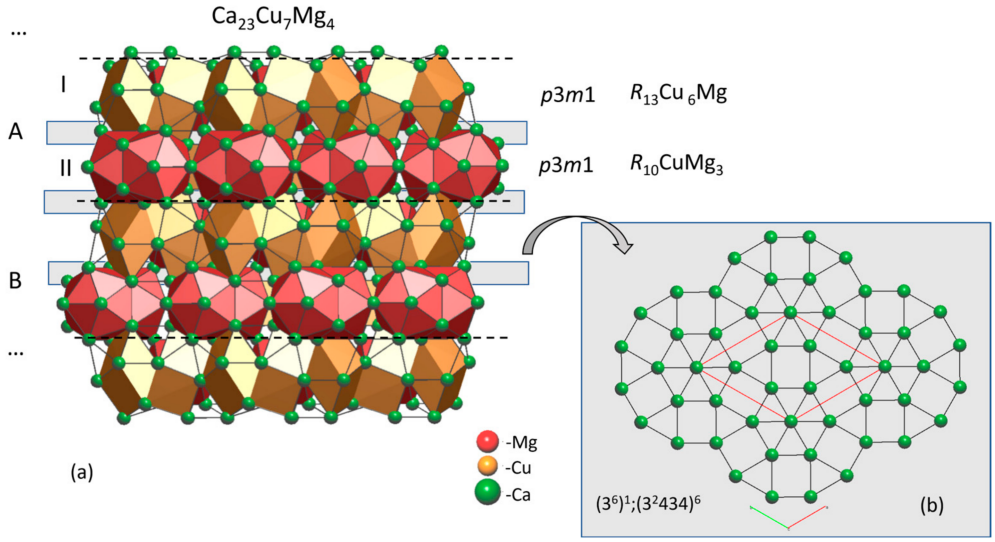

Figure 6. (**a**) Crystal structure of the $Ca_{23}Cu_7Mg_4$ as a. . .ABAB...sequence of identical double slabs, each composed of one $Ca_{13}Cu_6Mg$ (I) and one $Ca_{10}CuMg_3$ (II) single slab. The layer group symbol and thickness of each slab are indicated as well; (**b**) top view of a sewing layer with the corresponding Schläfli notation; red lines highlight the unit cell.

It should be noted that the $P6_3/mmc$ space group of title compounds is the only centrosymmetric one among the three hexagonal space groups compatible with the $p3m1$ layer symmetry of the stacked slabs [13]. Lattice parameters of representatives with the same slabs stacked along c should be related to those of the parent structures, with a and b being similar or integer multiples and c correlated to the total number of slabs in the unit cell. This is true for 23:7:4 and 4:1:1 compounds, having $a = b \approx 10$ Å and $c \approx 24$ Å and 51 Å, respectively.

The compositions of the two families of divalent R-rich compounds can be plotted on a Gibbs triangle, highlighting the relation with compositions of parent types (see Figure 7) and helping to develop the structural/compositional generalization idea. In fact, hypothetic new compounds with similar intergrowth architectures should show stoichiometries laying along the dotted tie-lines.

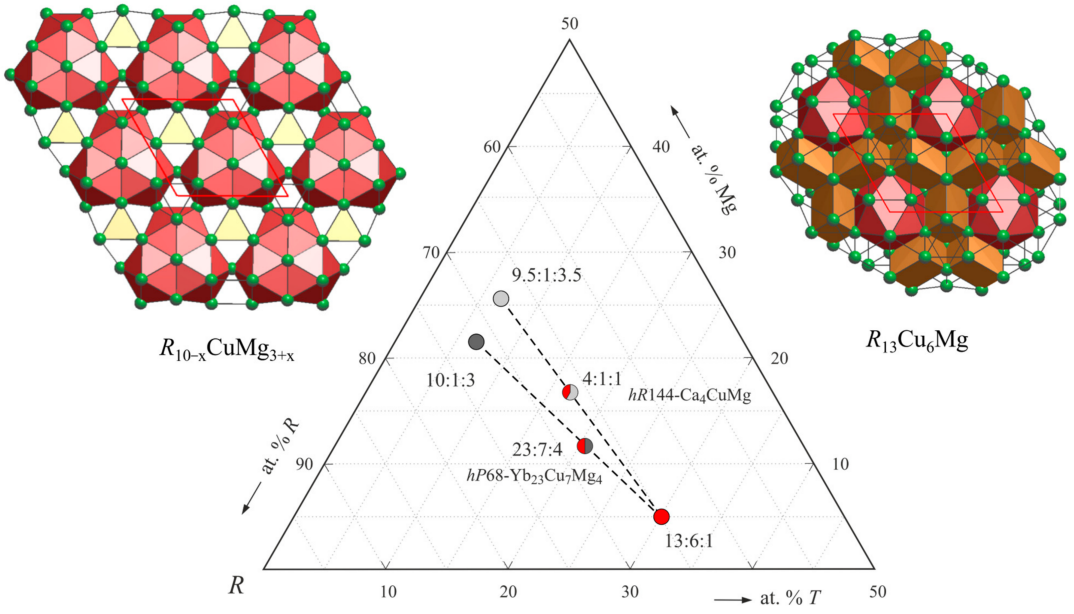

Figure 7. R_4CuMg and $R_{23}Cu_7Mg_4$ (R = Ca, Eu, Yb) compounds represented on a partial Gibbs triangle as combinations of stoichiometries corresponding to parent types (ends of dotted segments).

The specific compositions of the $R_{10-x}CuMg_{3+x}$ end member are indicated with different gray shadows. The amounts of end members in compounds of interest correspond to colored area ratios within the circles. Top views of the unique parent types of slabs are shown as well (red lines highlight the unit cell).

At this point, it is interesting to compare the two structural sub-families of $R_{23}T_7X_4$ intermetallics in terms of their component nature. A similar analysis was applied to R_4TMg using the volume contraction as a criterion. This is defined as $\Delta V_f(\%) = 100 \times \frac{V_{meas}-V_{calc}}{V_{calc}}$, where $V_{calc} = \sum_i N_i \times V_i$, ($N_i$ = number of i-type atoms in the unit cell, V_i = atomic volume of the i-type species taken from [24]) and V_{meas} is the experimentally determined volume [25]. The values of ΔV_f (%) for $R_{23}T_7X_4$ are plotted in Figure 8, as a function of the T group and of the R trivalent/divalent nature.

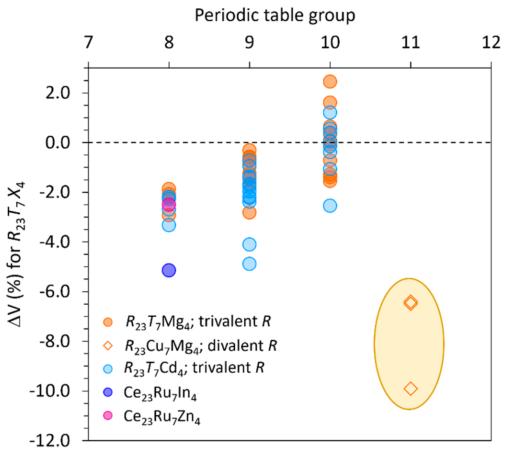

Figure 8. ΔV_f (%) for $R_{23}T_7X_4$ compounds. The dotted black line is an eye guide for the ideal Vegard's law behavior. A clear separation is visible between the hP68-$Pr_{23}Ir_7Mg_4$ and *hP*68-$Yb_{23}Cu_7Mg_4$ families of compounds.

A major part of ΔV_f (%) are negative, except for compounds with T = Pt, for which values lay in the range between 0 and +2.4%. No separation is observed as a function of X nature.

Instead, the title compounds, the only representatives known for divalent R, form a clearly clustered group, showing the most prominent volume contractions, extending down to −10% and indicating strong chemical interactions.

It is worth noting that both R and T nature are determinant for the formation and structure of these R-rich compounds; for example, the existence of $R_{23}T_7Mg_4$ has been excluded for several combinations of trivalent R with {Cu, Ag, Au} [2,26–28]. On the other hand, for T belonging to the 10th group (Ni, Pd, Pt) no representatives were found with divalent R so far. Considering the similar trend observed for the structurally related 4:1:1, these combinations are indeed worth investigating.

4. Conclusions

In this work, the crystal structures of the $\{Ca, Eu\}_{23}Cu_7Mg_4$ compounds were solved by single-crystal X-ray measurements, being the second and third representatives of the $Yb_{23}Cu_7Mg_4$ prototype and forming a small structural sub-family of 23:7:4 with a divalent R constituent. These few compounds are characterized by pronounced volume contractions if compared with the highly populated $R_{23}T_7X_4$ family with trivalent R having an $Pr_{23}Ir_7Mg_4$-type structure. The distribution in members of both groups discovered so far as a function of the nature of components, suggests combinations for new exploratory syntheses aiming to enrich the $Yb_{23}Cu_7Mg_4$-type representatives; for example $R_{23}\{Ag, Au\}_7Mg_4$, $R_{23}\{Ni, Pd, Pt\}_7Mg_4$ and $R_{23}Cu_7\{Zn, Cd, Al, In\}_4$ with R = Ca, Eu, Yb.

The crystal structure of the title compounds was interpreted in terms of linear intergrowth of slabs $R_{10}CuMg_3$ (parent type: *hP*28-kh^2ca, SG 194) and $R_{13}Cu_6Mg$ (parent type: *hR*60-b^6a^2, SG 160), alternating along the *c*-axis in the 1:1 ratio. This description brings together $\{Ca, Eu, Yb\}_{23}Cu_7Mg_4$ and $\{Ca, Eu, Yb\}_4CuMg$ compounds, the latter being formed by the same type of slabs in a 2:1 ratio. An evolution of this idea pushes towards the recognition/discovery of new structural families, based on different intergrowths of the same slabs. To this purpose, the following conditions should be fulfilled:

(1) Composition restraint—stoichiometries laying along the lines joining the end members;
(2) Symmetry restraint—rhombohedral, hexagonal and cubic space groups including the *p*3*m*1 among possible sd linear orbits [13,29];
(3) Metric restraint—for hexagonal and rhombohedral representatives $a = b \approx 10 \div 11$ Å or their multiples.

The results of the structural/chemical analysis illustrated here constitute a further step towards a planned, wider generalization aimed to a simple and chemically significant representation in terms of few common building blocks of complex *R*-rich ternary intermetallics.

Supplementary Materials: The following supporting information can be downloaded at: https://www.mdpi.com/article/10.3390/cryst14020156/s1, X-ray crystallographic files in CIF format.

Author Contributions: Conceptualization, P.S., S.D.N.; Methodology, P.S., R.F., S.D.N.; Investigation, P.S., R.F.; Data curation, R.F.; Writing – original draft, P.S., S.D.N.; Writing—review & editing, P.S., R.F., S.D.N.; Visualization, P.S. All authors have read and agreed to the published version of the manuscript.

Funding: This research received no external funding.

Data Availability Statement: The original contributions presented in the study are included in the article and Supplementary Materials, further inquiries can be directed to the corresponding author.

Conflicts of Interest: The authors declare no conflict of interest.

References

1. Solokha, P.; De Negri, S.; Pavlyuk, V.; Saccone, A. The novel intermetallic phases TbNiMg and $Tb_{4+x}Ni_2Mg_{3-x}$ (x = 0.2): Synthesis, crystal structure and peculiarities. *Intermetallics* **2010**, *18*, 719–724. [CrossRef]
2. Freccero, R.; De Negri, S.; Saccone, A.; Solokha, P. Solid state interactions in the La-Au-Mg system: Phase equilibria, novel compounds and chemical bonding. *Dalt. Trans.* **2020**, *49*, 12056–12067. [CrossRef] [PubMed]
3. Steurer, W.; Dshemuchadse, J. *Intermetallics: Structures, Properties, and Statistics*; Oxford University Press: Oxford, UK, 2016.
4. Villars, P.; Cenzual, K. *Pearson's Crystal Data: Crystal Structure Database for Inorganic Compounds*; ASM International: Materials Park, Ohio, USA, 2023.
5. Pöttgen, R. The Gd_4RhIn Type: Crystal Chemistry and Properties. *Handb. Phys. Chem. Rare Earths* **2020**, *58*, 1–38. [CrossRef]
6. Block, T.; Pöttgen, R. Cd3 and Cd4 Clusters in the Rare Earth (RE) Metal-Rich Phases $RE_{10}OsCd_3$ and RE_4OsCd. *Monatshefte Chem.* **2019**, *150*, 975–982. [CrossRef]
7. Block, T.; Stein, S.; Heletta, L.; Pöttgen, R. Osmium and magnesium: Structural segregation in the rare earth-rich intermetallics RE_4OsMg (RE = La-Nd, Sm) and RE_9TMg_4 (RE = Gd, Tb). *Z. Naturforsch. Sect. B J. Chem. Sci.* **2019**, *74*, 519–525. [CrossRef]
8. Tuncel, S.; Hermes, W.; Chevalier, B.; Rodewald, U.C.; Pöttgen, R. Ternary Magnesium Compounds $RE_{23}Ni_7Mg_4$ (RE = La, Ce, Pr, Nd, Sm) with $Pr_{23}Ir_7Mg_4$ Type Structure. *Z. Anorg. Allg. Chem.* **2008**, *634*, 2140–2144. [CrossRef]
9. Tappe, F.; Pöttgen, R. Rare Earth-Rich Cadmium Compounds $RE_{23}T_7Cd_4$ (T = Co, Ni, Ru, Rh, Ir, Pt). *Z. Naturforsch. Sect. B J. Chem. Sci.* **2009**, *64*, 184–188. [CrossRef]
10. Linsinger, S.; Eul, M.; Hermes, W.; Hoffmann, R.D.; Pottgen, R. Intermediate-Valent $Ce_{23}Ru_7Mg_4$ and $RE_{23}Ru_7Mg_4$ (RE = La, Pr, Nd) with $Pr_{23}Ir_7Mg_4$-Type Structure. *Z. Naturforsch. Sect. B J. Chem. Sci.* **2009**, *64*, 1345–1352. [CrossRef]
11. Bin, S.J.B.; Fong, K.S.; Chua, B.W.; Gupta, M. Mg-based bulk metallic glasses: A review of recent developments. *J. Magnes. Alloys* **2022**, *10*, 899–914. [CrossRef]
12. Luo, Q.; Gu, Q.F.; Zhang, J.Y.; Chen, S.L.; Chou, K.C.; Li, Q. Phase Equilibria, Crystal Structure and Hydriding/Dehydriding Mechanism of $Nd_4Mg_{80}Ni_8$ Compound. *Sci. Rep.* **2015**, *5*, 15385. [CrossRef] [PubMed]
13. Solokha, P.; Freccero, R.; De Negri, S. Architecture of new $\{Ca, Eu, Yb\}_4CuMg$ complex intermetallics based on polyicosahedral clusters. *J. Solid State Chem.* **2023**, *328*, 124353. [CrossRef]
14. Rodewald, U.C.; Tuncel, S.; Chevalier, B.; Pöttgen, R. Rare Earth Metal-Rich Magnesium Compounds RE_4IrMg (RE = Y, La, Pr, Nd, Sm, Gd, Tb, Dy) and $RE_{23}Ir_7Mg_4$ (RE = La, Ce, Pr, Nd). *Z. Anorg. Allg. Chem.* **2008**, *634*, 1011–1016. [CrossRef]

15. De Negri, S.; Saccone, A.; Rogl, P.; Giester, G. The ternary system Yb–Cu–Mg: Isothermal section at 400 °C in the range from 0 to 67 at.% Cu. *Intermetallics* **2008**, *16*, 1285–1291. [CrossRef]
16. Kraus, W.; Nolze, G. POWDER CELL—A program for the representation and manipulation of crystal structures and calculation of the resulting X-ray powder patterns. *J. Appl. Crystallogr.* **1996**, *29*, 301–303. [CrossRef]
17. Bruker. *APEX4, v2022.10-0*; Bruker: Billerica, MA, USA, 2022.
18. Bruker. *SAINT, v8.30*; Bruker: Billerica, MA, USA, 2012.
19. Bruker. *XPREP, v2014/2*; Bruker: Billerica, MA, USA, 2014.
20. Bruker. *SADABS, v2016/2*; Bruker: Billerica, MA, USA, 2016.
21. Sheldrick, G.M. *SHELXL-2019/1*; Program for the Crystal Structure Refinement; University of Göttingen: Göttingen, Germany, 2019.
22. Emsley, J. *The Elements*; Clarendon Press: Oxford, UK, 1998.
23. Galadzhun, Y.V.; Hoffmann, R.D.; Heletta, L.; Horiacha, M.; Pöttgen, R. The Lutetium-rich Indide $Lu_{13}Ni_6In$. *Z. Anorg. Allg. Chem.* **2018**, *644*, 1513–1518. [CrossRef]
24. Villars, P.; Daams, J.L.C. Atomic-environment classification of the chemical elements. *J. Alloys Compd.* **1993**, *197*, 177–196. [CrossRef]
25. Merlo, F.; Fornasini, M.L. Volume effects in rare earth intermetallic compounds. *J. Alloys Compd.* **1993**, *197*, 213–216. [CrossRef]
26. De Negri, S.; Giovannini, M.; Saccone, A. Constitutional properties of the La–Cu–Mg system at 400 °C. *J. Alloys Compd.* **2007**, *427*, 134–141. [CrossRef]
27. De Negri, S.; Solokha, P.; Saccone, A.; Pavlyuk, V. The Y-Cu-Mg system in the 0–66.7 at.% Cu concentration range: The isothermal section at 400 °C. *Intermetallics* **2009**, *17*, 614–621. [CrossRef]
28. De Negri, S.; Solokha, P.; Pavlyuk, V.; Saccone, A. The isothermal section of the La-Ag-Mg phase diagram at 400 °C. *Intermetallics* **2011**, *19*, 671–681. [CrossRef]
29. Kopský, V.; Litvin, D.B. (Eds.) *International Tables for Crystallography Volume E: Subperiodic Groups*; International Union of Crystallography: Chester, UK, 2010. [CrossRef]